Journal of Taibah University for Science

ISSN: (Print) (Online) Journal homepage: www.tandfonline.com/journals/tusc20

Conjugate entropy generation and heat transfer in a wavy walls' enclosure containing a suspension of dilute nano-encapsulated phase change material

Hakim S. Sultan Aljibori, Mehdi Ghalambaz, Ali Akremi, Obai Younis, Mehdi Fteiti, Manuel Baro & Faisal Alresheedi

To cite this article: Hakim S. Sultan Aljibori, Mehdi Ghalambaz, Ali Akremi, Obai Younis, Mehdi Fteiti, Manuel Baro & Faisal Alresheedi (2025) Conjugate entropy generation and heat transfer in a wavy walls' enclosure containing a suspension of dilute nano-encapsulated phase change material, Journal of Taibah University for Science, 19:1, 2465043, DOI: 10.1080/16583655.2025.2465043

To link to this article: https://doi.org/10.1080/16583655.2025.2465043

Published online: 17 Feb 2025.

JOURNAL OF TAIBAH UNIVERSITY FOR SCIENCE
2025, VOL. 19, NO. 1, 2465043
https://doi.org/10.1080/16583655.2025.2465043

Conjugate entropy generation and heat transfer in a wavy walls' enclosure containing a suspension of dilute nano-encapsulated phase change material

Hakim S. Sultan Aljibori[a], Mehdi Ghalambaz [b,c], Ali Akremi[d], Obai Younis[e,f], Mehdi Fteiti[g], Manuel Baro [h] and Faisal Alresheedi[i]

[a]College of Engineering, University of Warith Al-Anbiyaa, Karbala, Iraq; [b]Department of Mathematics, Saveetha School of Engineering, SIMATS, Chennai, India; [c]Institute of Research and Development, Duy Tan University, Da Nang, Vietnam; [d]Department of Chemistry, Faculty of Science, Northern Border University, Arar, Kingdom of Saudi Arabia; [e]Department of Mechanical Engineering, College of Engineering in Wadi Addwasir, Prince Sattam Bin Abdulaziz University, Wadi Addawaser, Saudi Arabia; [f]Department of Mechanical Engineering, Faculty of Engineering, University of Khartoum, Khartoum, Sudan; [g]Physics Department, Faculty of Science, Umm Al-Qura University, Makkah, Saudi Arabia; [h]Researcher at the Tecnológico Nacional de México Campus Nuevo Casas Grandes, Nuevo Casas Grandes, México; [i]Department of Physics, College of Science, Qassim University, Buraidah, Saudi Arabia

ABSTRACT

The present article numerically investigated the conjugate heat transmission and entropy production of NEPCM enclosed within a cavity. The cavity was modified by inserting wavy blocks on both the top and bottom sides. The left and right borders of the wavy block are exposed to deferential heating, but the rest of the cavity walls are thermally insulated. The equations governing the system were analyzed utilizing Galerkin's weighted finite element method. The findings revealed that manipulating the wave amplitude to higher levels and decreasing the wavelength had a diminishing effect on heat transfer and entropy generation. Conversely, elevating both the Ra and R_k values resulted in a notable rise of up to 66% in the average Nusselt number (Nu_{avg}). Employing the optimal values of $\varphi = 0.05$ and $\theta_f = 0.5$ led to a 12% increase in Nu_{avg} and a 33% decrease in entropy production.

ARTICLE HISTORY
Received 5 January 2024
Revised 30 July 2024
Accepted 6 February 2025

KEYWORDS
phase change material; fusion temperature; conjugate free convection; entropy

1. Introduction

In the vast field of thermal management, a breakthrough technology is reshaping the way we perceive and utilize heat transfer: Nano-Encapsulated Phase Change Material (NEPCM) [1]. At the intersection of nanotechnology and thermodynamics, these advanced materials harness the transformative abilities of phase change materials (PCMs) but augment their potential by encapsulating them within nanoscale structures. This encapsulation not only ensures uniform dispersion in various mediums but also amplifies the inherent properties of PCMs, leading to enhanced heat absorption and release rates. NEPCM suspensions represent a cutting-edge solution to age-old challenges in various sectors, from electronics cooling to building temperature regulation and solar photothermal absorption and storage [2]. Investigating their underlying principles, applications, and future prospects offers a glimpse into a future where heat transfer is more efficient, adaptable, and sustainable than ever before. Huang et al. [3] discussed some encapsulation techniques of PCMs. Besides, PCMs have found applications in energy storage systems [4,5].

Heat transfer in enclosures plays an essential role in many engineering and scientific applications. The efficiency, safety, and performance of numerous devices and processes depend on the precise understanding and management of heat transfer within confined spaces. One of the most significant modes of fluid flow and heat transfer within these spaces is natural convection [6,7]. Natural convection occurs when fluid motion is induced by buoyancy forces, which arise due to temperature differences within the fluid. Unlike forced convection, where external mechanisms like fans or pumps drive fluid flow, natural convection relies on inherent fluid properties and external conditions.

A plethora of studies have explored natural convection within enclosures, particularly focusing on natural convection in rectangular cavities [6,7]. These studies incorporate both numerical simulations and experimental techniques to understand the intricate dynamics at play. By examining various formations of the enclosures – differing in initial and boundary conditions, locations of heat sources [8], and radiative characteristics of the medium [9] and walls – researchers have sought to comprehend how parameters like the cavity tilt angle, Prandtl and Rayleigh numbers, and surface emissivity [10], and thermal properties affect heat transfer dynamics [6,7].

CONTACT Mehdi Ghalambaz ghalambaz.mehdi@gmail.com; mehdighalambaz@duytan.edu Ali Akremi ali.akrmi@nbu.edu.sa

Moreover, understanding natural convection in non-rectangular enclosures is equally vital. Enclosures of different shapes, including the parallelogrammical diode cavity [11], enclosures with inner bodies [12,13], wavy cavities [14,15], and U-shape enclosures [16] have been examined to explore their unique heat transfer characteristics. These works highlight the broad range of scientific and technical disciplines in which understanding free convective flow in cavities proves beneficial.

Conjugate heat transfer, a phenomenon that couples different modes of heat transfer, like conduction, convection, and radiation in a composite medium, has garnered considerable attention in the context of enclosures or cavities [17,18]. Alhashash and Saleh [19] studied the enhancement of conjugate heat transfer in an enclosure with an active cylinder placed in the centre. It was revealed that the space between the cylinder and the enclosure walls could significantly influence heat transfer. The role of the cylinder's rotational direction in dictating peak Nusselt number values underscores the intricate balance of factors involved in optimizing heat transfer in such systems. Further, an exploration into the conjugate heat transfer in an inclined blocked square enclosure brought out the profound effects of factors like the inclination angle and block thermal conductivity ratio [20]. Interestingly, an inclination angle from 0° to 90° showed a remarkable enhancement in the average Nusselt number, especially at higher Rayleigh numbers.

Conjugate heat transfer also found applications in the field of magnetohydrodynamics. The investigation of an aqueous hybrid nano-liquid confined within concentric cylinders under the influence of magnetic fields shown that such hybrid nano-liquids have the potential to promote improved thermal dissipation from the interface between a solid and a fluid within an annular region [21]. Additionally, when addressing MHD conjugate natural convection and entropy generation in a square enclosure, it was found that the position of heat-generating elements could greatly impact thermal performance [22].

Entropy generation, an indicator of irreversibility in thermodynamic processes, plays a pivotal role in understanding and optimizing heat transfer processes. In the context of enclosures, thermal-fluid flow in cylinder-embedded annular systems revealed that entropy generation contours tend to concentrate near heated and cooled walls at higher buoyant forces [23]. Furthermore, a review of Newtonian and non-Newtonian nanofluids emphasized the significance of understanding entropy generation in hybrid nanofluid-porous enclosures, underlining the vast applications in areas like nuclear reactors and cooling systems [24].

Entropy generation's nuanced behaviour was further demonstrated in a square enclosure using Cu/water nanofluid, with findings indicating that global entropy generation could decrease when increasing the nanoparticle volume fraction at a certain Ra [25]. A distinct research focused on analyzing non-Newtonian nanofluid free convection occurring within a tilted U-shaped container, which also incorporated a heated structure resembling a tree as a baffle. This study underscored the critical role of optimizing entropy in a range of thermal systems [16].

Heat transfer in wavy-walled enclosures or cavities has been a focus of several research studies [26]. The wavy geometry of the cavity walls tends to significantly influence the convection behaviour and, subsequently, the heat transfer rates. Recent computational studies have explored various aspects of this subject, shedding light on the intricate patterns and behaviours induced by undulations or waves in the enclosure walls. Fayz-Al-Asad et al. [27] revealed that undulations on the walls could amplify the heat transport within a cavity, especially when the number of waves increases, thus influencing the convection patterns and heat distribution. Notably, the research found that heat transport escalated with an increase in both the Rayleigh number and the number of undulations. Another study investigated the effect of inclined wavy walls on nanofluids, highlighting that changes in the wall patterns resulted in significant alterations in temperature and entropy profiles within the enclosure [28]. A study on magnetohydrodynamic natural convection in a wavy enclosure with a circular hot cylinder inside underscored the role of heat generation and absorption in the process [29]. The results indicated that higher Rayleigh numbers and certain heat coefficients could either enhance or dampen the Nusselt number, a primary metric for convective heat transfer.

Furthermore, studies have ventured into non-Darcian porous wavy enclosures, demonstrating that changing certain variables like the undulation amplitude and the Rayleigh number can have pronounced effects on flow strength and heat transfer efficiency [30]. An intriguing observation was made in a study exploring an I-shaped wavy-walled enclosure, which found that a single undulation was the optimal configuration for enhanced heat transfer [31]. Lastly, when non-Newtonian ferrofluids are considered in a wavy enclosure under a magnetic field, the rheology of the fluid becomes a critical factor. Depending on whether the fluid exhibits shear-thinning or shear-thickening behaviour, the heat transfer rates and flow dynamics can vary considerably [32].

The nature of the working fluid inside the enclosure also influences the heat transmission dynamics. Incorporating nanofluids, for instance, can modify the natural convection patterns, offering potential enhancements in heat transfer rates [33]. This adaptation highlights the evolving nature of heat transfer research, constantly seeking ways to optimize and improve upon existing knowledge.

Some recent researchers investigated the convection heat transfer of NEPCM suspensions in enclosures. When placed in an enclosure, NEPCMs are pivotal in managing heat transfer. One investigation showed that, in a square cavity with differentially heated vertical walls, the NEPCM particles undergo a phase change, absorbing latent heat in hot regions and releasing this absorbed heat in the cold areas through solidification [34]. This dynamic process can lead to heat transfer enhancements of around 10% compared to base fluids. The fusion temperature of these particles remains a critical factor, indicating the potential of NEPCMs in specific temperature ranges to optimize their performance. Various research has employed distinct geometries in order to examine the impact of NEPCMs on heat transmission. An experimental setup using a compound cavity, consisting of a centre circular cylinder mixed with rectangular forms, was utilized in previous research to investigate the phenomenon of double-diffusive convection in NEPCMs [29]. The temperature at which fusion occurs had a significant role in shaping the spatial distribution and magnitude of phase transition regions. In a separate experimental configuration, a porous grooved cavity was utilized to investigate the phenomenon of natural convection in a water-based suspension of NEPCMs [30]. Variables such as the Darcy parameter, Rayleigh number, and fusion temperature emerged as significant parameters influencing convection patterns and heat transfer. Another recent study shows the significance of the Rayleigh number on heat transfer and entropy production [35]. Besides, the exothermic reaction of NEPCMs has been addressed by Pasha et al. [36]. Other aspects of NEPCM suspensions such as bioconvection and oxytactic microorganisms [37], micro-polar NEPCMs [38] have been investigated as well.

The complexity and versatility of NEPCM applications are evident in a study involving two differently heated circular cylinders in an adiabatic enclosure [36]. Results from this study unveiled that adjusting parameters like the Stefan and Rayleigh numbers could result in significant variations in heat transfer rates. Additionally, the proximity of the fusion temperature to the cylinders' temperatures can have implications on the overall heat transfer. Adding to the myriad of studies, the introduction of solid particles into NEPCMs to boost their thermal performance has also been explored [39]. In a hexagonal-shaped cavity with rotating super ellipse shapes, different variables were found to influence heat and mass transport. Furthermore, considering the entropy in the flow of NEPCMs reveals the intricacies of radiative heat transfer and the interaction between radiation and convective modes [40]. Using NEPCMs in prismatic enclosures filled with isotropic porous media can significantly enhance heat transfer while influencing melting and solidification processes.

The literature review highlights a crucial focus on entropy generation and heat transfer phenomena within wavy enclosures for nanofluids and other working fluids as subjects extensively investigated by scholars. In this landscape, NEPCM suspensions stand out as groundbreaking heat transfer fluids, poised to revolutionize thermal management through nanoparticle-induced phase change. Leveraging the distinctive phase transition properties of NEPCM suspensions, the intricate heat transfer dynamics of these advanced nanofluids demand thorough investigation. This study boldly embarks on pioneering the analysis of conjugate heat transfer and entropy generation within a wavy enclosure employing NEPCM suspensions, aiming to unravel their complex interplay and potential for enhanced thermal performance.

Table 1. Details the thermophysical attributes of the materials under consideration, as cited from references [41,42].

Material	ρ (kg/m^3)	C_p (J/kg.K)	k (W/m.K)	β (K^{-1})	μ (kg/m.s)
Nonadecane	721	2037	–	–	–
Polyurethane	786	1317.7	–	17.28×10^{-5}	–
Host fluid (water)	997.1	4179	0.613	21×10^{-5}	8.9×10^{-4}

2. Problem physics

This study examines a two-dimensional cavity featuring an affixed solid wavy wall, as illustrated in Figure 1. The wavy block's side boundaries are kept heated and cooled, with temperatures set at T_h and T_c correspondingly. In contrast, the remaining enclosure walls are efficiently insulated. The enclosure's empty region is loaded with a mixture of water and NEPCM particles, which move due to natural convection. The wavy solid blocks were introduced using the following relation: $y = a \times \sin(2\pi x/\Omega)$. Where a and Ω are respectively, the wave amplitude and wavelength. The wavy wall structure provides increased surface for heat transfer and also improved mechanical structure for enclosures. The wavy surface enclosures have applications in solar collectors and water purification systems.

The thermophysical characteristics of the core component (nonadecane), the base fluid (water), and the encapsulating layer (polyurethane) are detailed in Table 1. As per reference [41], nonadecane has a fusion temperature close to 32 °C and a latent heat of approximately 211 kJ/kg.

2.1. Governing equations

The suspension is treated as uniform with no assumed thermal or hydrodynamic slippage. The nanoparticles are in thermal equilibrium with the host fluid and there is no degradation in the nanofluid uniformity; besides, the nanoparticles do not react with the host fluid. By applying Boussinesq's approximation, which accounts for density variations due to buoyancy in modelling a

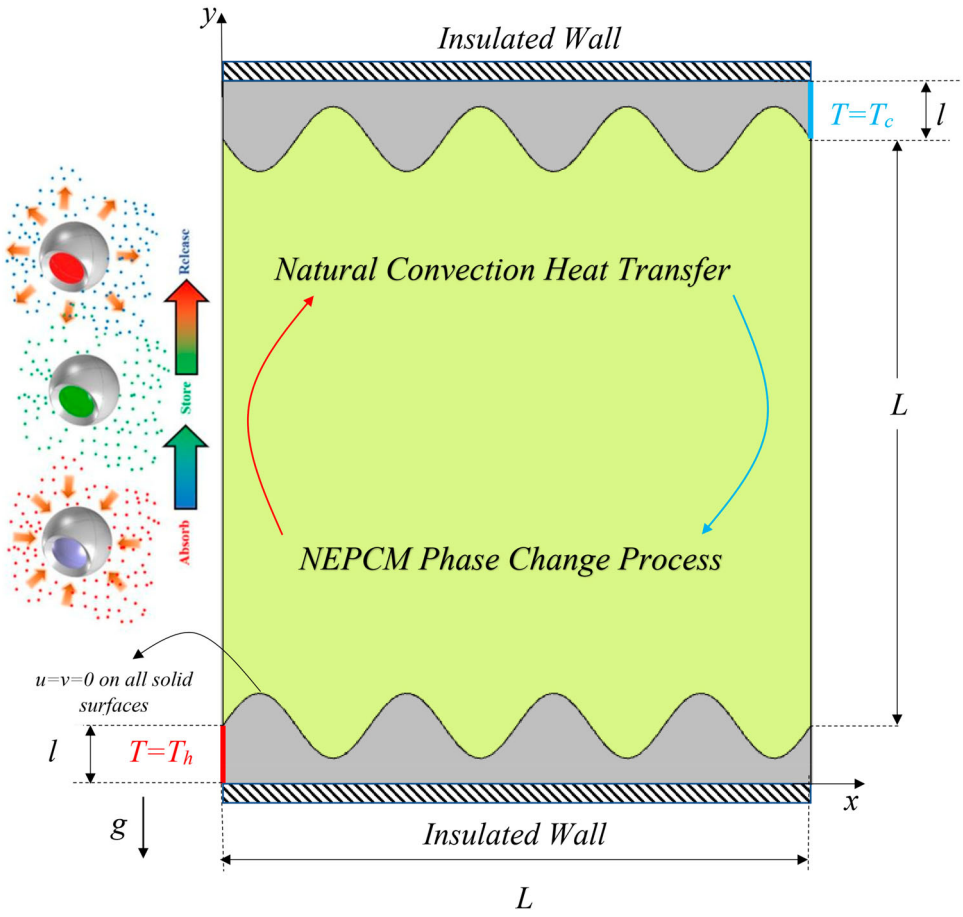

Figure 1. The computational domain and applied boundary conditions.

laminar, steady, and incompressible flow, the hydrodynamic and thermal characteristics of the NEPCM-inclusive suspension can be articulated as [34,43,44]:

Mass conservation

$$\nabla^* \mathrm{u} = 0 \tag{1}$$

Conservation of momentum

$$\rho_{npcm}[(\mathrm{u}.\nabla^*)\mathrm{u}] = -\nabla^* p + (\mu_{npcm}\nabla^{*2}\mathrm{u}) + \mathrm{f_B} \tag{2}$$

Energy conservation

$$(\rho Cp)_{npcm}[\mathrm{u}.\nabla^* T] = k_{npcm}(\nabla^{*2} T) \tag{3}$$

where the buoyancy force ($\boldsymbol{f_B}$) is introduced as:

$$\mathrm{f_B} = \begin{cases} x: & 0 \\ y: & \rho_{npcm}\beta_{npcm} g(T - Tc) \end{cases} \tag{4}$$

Conduction heat transfer in solid wavy blocks:

$$k_{Block}(\nabla^{*2} T) = 0 \tag{5}$$

where ρ, Cp, β, k, and μ indicate the density, heat capacity per unit of mass, thermal volume expansion, thermal conductivity, and dynamic viscosity, respectively. The subscripts *npcm* and *Block* denote the suspension and solid wall. The gravity is represented by g. The field variables T and p denote the temperature and pressure, while $\boldsymbol{u}$ shows the velocity vector for suspension. Considering the boundary conditions, the continuity of heat flux and temperature was applied at the wavy interface of the wall and NEPCM suspension. The isotherm temperatures of $T = T_c$ and $T = T_h$ were applied at the hot and cold portions of the wavy wall block. The zero-heat flux was applied to the other walls. The zero velocity was applied to all walls exposed to the NEPCM suspensions. A zero-reference pressure was also considered at the bottom left corner of the enclosure in the fluid domain.

2.2. Physical relationships for the suspension

The density of the suspension is calculated through a weighted function incorporating both the dispersed nanoparticles and the host fluid [45]. Here, subscripts *np* and *f* signify the nanoparticles and host fluid, respectively:

$$\rho_{npcm} = \rho_f(1 - \varphi) + \varphi\rho_{np} \tag{6}$$

For NEPCMs, the density can be computed using the following equation, where subscripts *c* and *s* correspond to the densities of the core and shell, respectively [45,46]:

$$\rho_{np} = \frac{\rho_s\rho_c(1 + \iota)}{\rho_s + \rho_c\iota} \tag{7}$$

The weight ratio ι between the core and the shell for the materials under study is approximately 0.447 [41]. The

heat capacity of the suspension is computed using the equation below [46,47]:

$$C_{p,npcm} = \frac{\rho_f C_{p,f}(1-\varphi) + \rho_{np} C_{p,np}\varphi}{\rho_{npcm}} \tag{8}$$

For the overall heat capacity and by considering the phase change in the nanoparticle core, a sinusoidal profile is proposed [45,48]:

$$C_{p,np} = C_{p,c} + \frac{\pi}{2}\left\{\left(\frac{h_{sf}}{\delta T} - C_{p,c}\right)\sin\left(\pi\frac{T - T_{solid}}{\delta T}\right)\right\} \times \begin{cases} 0 & T < T_{solid} \\ 1 & T_{solid} < T < T_{liquid} \\ 0 & T > T_{liquid} \end{cases} \tag{9}$$

In this context, the temperature interval $\delta T = T_{\text{liquid}}$-$T_{\text{solid}}$ is defined as in which T_{liquid} and T_{solid} are the temperatures of the solid and liquid core nanoparticles. Here, $T_f = (T_{\text{liquid}} + T_{\text{solid}})/2$ is the phase change temperature of the nanoparticle's core. The suspension's volumetric thermal expansion coefficient is given by the following expression [47]:

$$\beta_{npcm} = \beta_f(1-\varphi) + \beta_{np}\varphi \tag{10}$$

The suspension's thermal conductivity and dynamic viscosity are determined using linear relationships, as shown below [49,50]:

$$\frac{k_{npcm}}{k_f} = Nc\varphi + 1 \tag{11}$$

$$\frac{\mu_{npcm}}{\mu_f} = Nv\varphi + 1 \tag{12}$$

Here, Nv and Nc denote the numerical coefficients, which can be determined using experimental data such as those reported in [41].

2.3. Suspensions streamlines and entropy generation

The flow characteristics of the suspension can be illustrated using the contours of the streamlines (ψ). The streamlines are established based on the components of velocity, represented as:

$$\begin{cases} v = -\dfrac{\partial\psi}{\partial x} \\ u = \dfrac{\partial\psi}{\partial y} \end{cases} \tag{13}$$

and the streamline function is introduced as:

$$\nabla^{*2}\psi = \left(\frac{\partial u}{\partial y} - \frac{\partial v}{\partial x}\right) \tag{14}$$

Applicable boundary conditions for this equation are uniformly defined across all boundaries with zero streamline value. Entropy generation in the flow is influenced by two primary factors: thermal and frictional entropy. This is mathematically described by [51]:

$$s_{local} = \frac{k_{npcm}}{T_0^2}\left[\left(\frac{\partial T}{\partial y}\right)^2 + \left(\frac{\partial T}{\partial x}\right)^2\right] + \frac{\mu_{npcm}}{T_0}\left(\left(\frac{\partial v}{\partial x} + \frac{\partial u}{\partial y}\right)^2 + 2\left(\left(\frac{\partial v}{\partial y}\right)^2 + \left(\frac{\partial u}{\partial x}\right)^2\right)\right) \tag{15}$$

In this equation, the first term corresponds to entropy generation due to thermal gradients, while the second term accounts for the entropy induced by friction between fluid layers.

2.4. Applied boundary conditions

The no slip and no permeability were applied to all fluid exposed surfaces. The continuity of heat flux and temperature are also applied to the conjugate interfaces between the fluid and solid blocks. The zero heat-flux was applied to the bottom and top walls, representing insulations, while the indicated portion of sidewall blocks were kept at isothermal temperatures T_c and T_h. A zero reference-pressure point was considered at the beginning of the wavy wall at the top.

2.5. Dimensionless formulation

To render governing equations and the boundary conditions into dimensionless equations, the normalization parameters are introduced as:

$$X = \frac{x}{L},\ Y = \frac{y}{L},\ \nabla^* = \frac{\nabla}{L},\ l_1 = \frac{l}{L},$$
$$A = \frac{a}{L},\ V = \frac{vL}{\alpha_f},\ U = \frac{uL}{\alpha_f},$$
$$P = \frac{pL^2}{\rho_f\alpha_f^2},\ \Psi = \frac{\psi}{\alpha_f},$$
$$\theta = \frac{T - Tc}{\Delta T},\ \theta_f = \frac{T_f - T_c}{\Delta T},\ \lambda = \frac{\Omega}{2\pi L} \tag{16}$$

and $\Delta T = T_h$-T_c. This leads to the following dimensionless equations:

$$\nabla U = 0 \tag{17}$$

$$\frac{\rho_{npcm}}{\rho_f}[(U.\nabla)U] = -\nabla P + \Pr\frac{\mu_{npcm}}{\mu_f}\nabla^2 U + F_B \tag{18}$$

$$Cr[U.\nabla\theta] = \frac{k_{npcm}}{k_f}(\nabla^2\theta) \tag{19}$$

$$R_k(\nabla^2\theta) = 0 \tag{20}$$

where

$$F_B = \begin{cases} X: & 0 \\ Y: & \frac{\rho_{npcm}}{\rho_f}\frac{\beta_{npcm}}{\beta_f} Ra \Pr \theta \end{cases} \quad (21)$$

$$Cr = \frac{(\rho Cp)_{npcm}}{(\rho Cp)_f} = \lambda_0 \varphi + \frac{\varphi}{Ste \times \delta} f + (1-\varphi) \quad (22)$$

$$f = \sin\left(\frac{\pi}{\delta}\left(\theta + \frac{\delta}{2} - \theta_f\right)\right)\frac{\pi}{2} \times \begin{cases} 0 & \theta < (\theta_f - \delta/2) \\ 1 & (\theta_f - \delta/2) < \theta < (\theta_f + \delta/2) \\ 0 & \theta > (\theta_f + \delta/2) \end{cases} \quad (23)$$

and

$$Pr = \frac{\mu_f}{\alpha_f \rho_f},\ Ra = \frac{\beta_f \rho_f \Delta T L^3 g}{\mu_f \alpha_f},\ R_k = \frac{k_{Block}}{k_f} \quad (24)$$

$$\lambda_0 = \frac{(Cp_{s1} + Cp_{c,l})\rho_s \rho_c}{(\rho_c \iota + \rho_s)(\rho Cp)_f},\ \delta = \frac{\delta T}{\Delta T},$$

$$Ste = \frac{(\rho_c \iota \rho_s)(\rho Cp)_f \Delta T}{(\rho_s \rho_c h_{sf})\alpha_f} \quad (25)$$

The wavy wall formula scales to $Y = A \times \sin(X/\lambda)$, where A and λ are the dimensionless wave amplitude and wavelength, respectively. Besides, the density ratio $\rho_R = \rho_{np}/\rho_f = 0.74$ and $\rho_{npcm}/\rho_f = (1\text{-}\varphi) + \varphi \times \rho_R$.

The streamline and entropy generation are obtained as follows:

$$\nabla^2 \Psi = \left(\frac{\partial U}{\partial Y} - \frac{\partial V}{\partial X}\right) \quad (26)$$

The dimensionless local entropy production ($S_{T,local}$) is expressed as

$$S_T = \frac{k_{npcm}}{k_f}\left[\left(\frac{\partial \theta}{\partial Y}\right)^2 + \left(\frac{\partial \theta}{\partial X}\right)^2\right]\chi_0 \frac{\mu_{npcm}}{\mu_f} + \left(\left(\frac{\partial U}{\partial Y} + \frac{\partial V}{\partial X}\right)^2 + 2\left(\left(\frac{\partial U}{\partial X}\right)^2 + \left(\frac{\partial V}{\partial Y}\right)^2\right)\right) \quad (27)$$

where the irreversibility parameter (χ_0) is:

$$\chi_0 = \left(\frac{\alpha_f}{\nabla T \times L}\right)^2 \frac{T_f \mu_f}{k_f} \quad (28)$$

2.6. Heat transfer rate and total entropy generation

The heat transfer rate at the hot wall is characterized by the local Nusselt number as:

$$Nu_Y = -R_k\left(\frac{\partial \theta}{\partial X}\right)_{@Hotwall} \quad (29)$$

$$Nu_{avg} = \int_0^{l_1} Nu_Y dY \quad (30)$$

$$S_T = \iint_A s_{T,local} dA \quad (31)$$

where A is the surface area of the domain.

Table 2. Influence of the mesh elements on Nu_{avg}.

Case No.	Sm	Elements	Nu_t	Err (%)
1	0.5	5194	1.2974	1.4
2	1	15706	1.3132	0.2
3	**1.5**	**29080**	**1.3212**	**0.4**
4	2	49772	1.3190	0.2
5	2.5	76306	1.3160	–

∗Bold row is the selected mesh for computations.

3. Solution method and verification

3.1. Numerical method

Galerkin's weighted finite element method was deployed to numerically address the dimensionless governing equations – namely, Equations (17)–(20). The computational domain was discretized using an unstructured mesh, with a particular focus on grid density in regions adjacent to solid boundaries. This was done to accurately capture rapid changes in both velocity and temperature profiles. To ensure full coupling of the discretized governing equations, the damped Newton method was applied. A damping value of 0.8 was applied for better convergence. The ensuing system of linear algebraic equations was then solved through the use of the Parallel Sparse Direct Solver. The computations were halted when the relative error reaches below 10^{-4}. For a comprehensive explanation of the numerical methods employed, please refer to [52]. After the computation of the flow field and temperature distribution entropy generation and heat transfer at the walls were calculated. A continuous approach for study of a range of parameters was applied. In this approach, as the value of a control parameter changes step by step, the solution for a parameter at a previous step was used as an initial guess for the next step.

3.2. Grid check

To ensure a grid-independent solution, a grid sensitivity analysis was performed in the current study. A variety of five non-uniform grid sizes were assessed to determine the most suitable mesh for accurate computational results. Table 2 details these cases and measures the relative errors against Case 5 as a baseline. In an additional layer of scrutiny, temperature distribution profiles along the cavity's vertical centreline for each of these five grid sizes are illustrated in Figure 2.

Table 2 provides a comprehensive evaluation of how different mesh sizes influence the calculated average Nusselt number measured at the hot vertical wall. Each case is subjected to specific conditions: Ra = 10^6, Pr = 6.2, δ = 0.05, R_k = 10, Ste = 0.3, θ_f = 0.3, Nc = 6, φ = 0.05, Nv = 3, λ_0 = 0.332, and l_1 = 0.1. The table further quantifies the relative error percentages, benchmarked against the values obtained in Case 5. Importantly, as the number of mesh elements

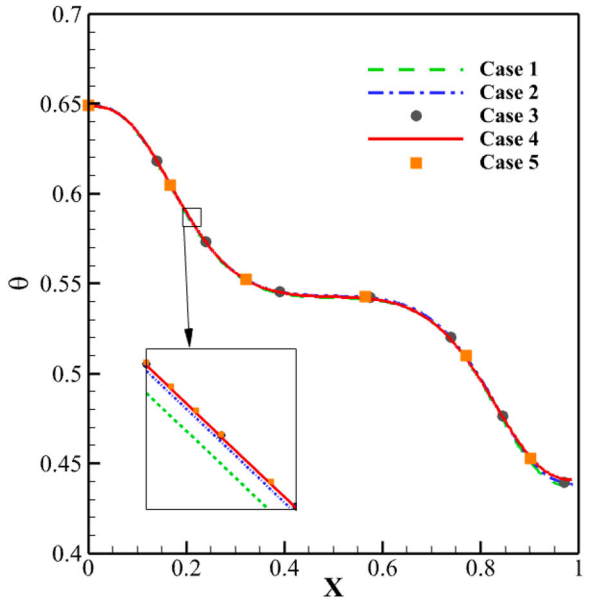

Figure 2. Temperature along X coordinate at mid-plane of the enclosure at $Y = 0$ for various examined meshes.

Table 3. The findings of Kahveci [53] and current research for average Nusselt number ($Ra = 10^6$).

Nu_{avg}	$\varphi = 0.0$	$\varphi = 0.05$	$\varphi = 0.1$
Kahveci [53]	9.23	9.77	10.23
Current research	9.20	9.76	10.30

increases, the error generally decreases, indicating a convergence towards a more accurate solution.

The performance metrics, specifically the average Nusselt number and the maximum velocity within the cavity, are reported for each grid size under the mentioned conditions. Balancing computational resource demands with the requirement for numerical accuracy, Case 3 – featuring 29,080 mesh elements – was chosen as the optimal grid size for subsequent analysis. This case computes the results with less than 1% which is adequate for most of graphical representations. It also provides a good convergence since the mesh is adequately fine. Figure 3 provides a view of the utilized mesh in the solution domain.

3.3. Validation and code verification

To substantiate the numerical accuracy of the finite element code employed in this study, comparisons have been made between the results obtained here and those published in prior works [53–56]. Table 3, as well as Figures 4 and 5, showcase these comparative analyses.

Specifically, Table 3 contrasts the average Nusselt numbers from this study with those presented in reference [53]. The latter work explored buoyancy-driven convective flow inside a square cavity loaded with a water-TiO2 nanoparticle suspension featuring isothermally heated vertical walls and insulated horizontal walls.

For additional verification, the temperature profiles generated by our numerical code for fluid flow in a square enclosure are compared against the results of the study of Turan et al. [54], as illustrated in Figure 4. Furthermore, Figure 4 plots the entropy fields of the present work alongside those presented in [55].

Figure 5 provides a comparison between our results and those published in [34] for an NEPCM suspension. The isotherms, phase transition (Cr) maps and streamlines are compared. As seen, a good match between the results can be found. Additionally, a comparative analysis was conducted between the findings of reference [57] and the current simulations on heat transfer involving two square cylinders in Figure 6. In this setup, the outer vertical walls were maintained at cold temperatures, while the left inner vertical wall was heated. The remaining walls were insulated. The aspect ratio (L) of the cylinders was set at 0.3.

4. Results and discussions

In this study, we evaluate both conjugate free convection and heat transmission, as well as the rate at which entropy is generated within an enclosure filled with a water-based suspension of NEPCMs particles. Several non-dimensional parameters are considered to characterize the system: these include the Rayleigh number (Ra) ranging from 10^3 to 10^5, the non-dimensional amplitude of wavy blocks A between 0.01 and 0.06, non-dimensional wave length (λ) from 0.25 to 0.75, and the non-dimensional fusion temperature (θ_f) from 0.1 to 0.9. Additional parameters include the thermal conductivity ratio (R_k) between 1 and 20 and the concentration of NEPCMs particles (φ) between 0.0 and 0.05.

Contrastingly, specific parameters are kept constant throughout the simulations: namely, $\chi_0 = 10^{-4}$, $\delta = 0.05$, $Pr = 6.2$, $Nc = 6$, $Nv = 6$, $l_1 = 0.1$, $\lambda_0 = 0.322$, and $Ste = 0.3$. For the purpose of this study, default values for variable parameters have been set as follows: $\theta_f = 0.3$, $\varphi = 0.05$, $Ra = 10^5$, $A = 1/18$, $\lambda = 0.25$, and $R_k = 10$.

This framework allows for a thorough examination of the thermofluidic phenomena within the enclosure, providing valuable insights into the roles of various parameters in affecting entropy generation and free convection.

The analysis presented in Figure 7 explores the complex relationship between the wave amplitude (A), the average Nusselt number (Nu_{avg}), and the overall entropy generation in a system subject to varying wavelength parameters (λ). The study reveals that an escalation in wave amplitude leads to a notable decrease in the rate of heat transfer, as indicated by the diminishing values of Nu_{avg}. This decline becomes even more

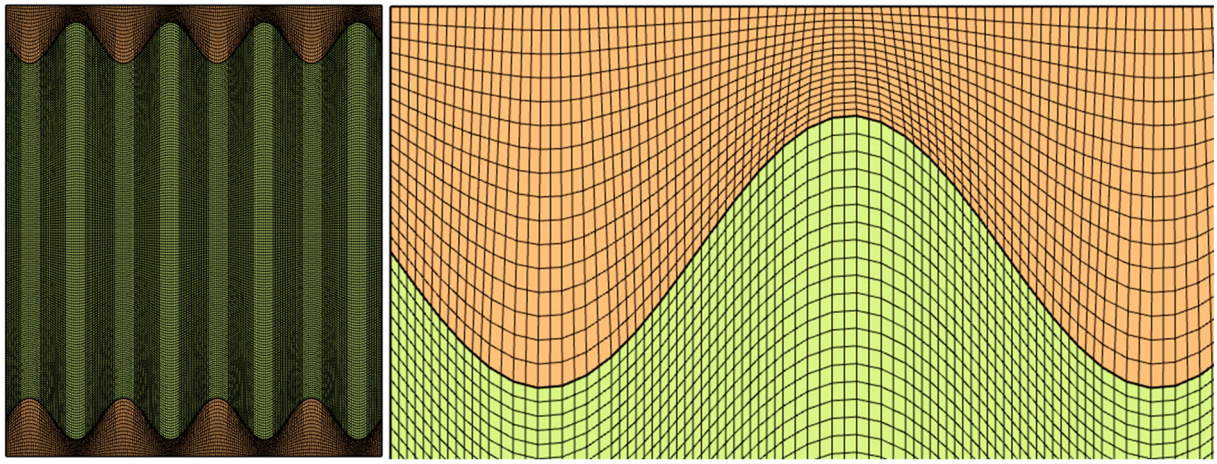

Figure 3. A view of utilized mesh: (a) overall view of the mesh, and (b) a zoomed view at the top left corner.

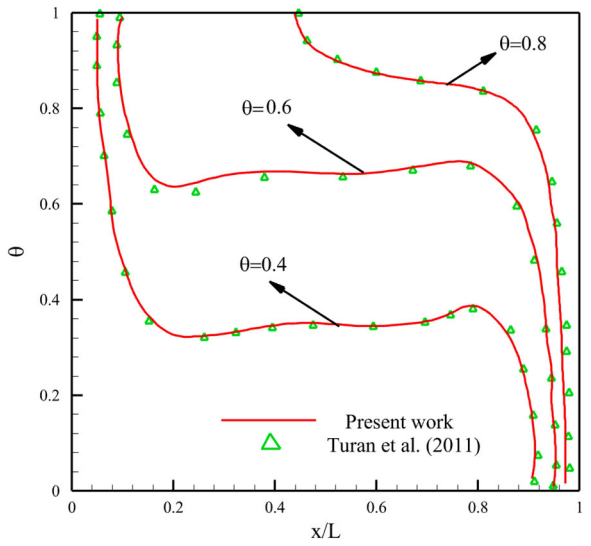

Figure 4. Isotherms evaluated in our study and those obtained by Turan et al. [54].

pronounced when the system operates at shorter wavelengths, corresponding to a higher frequency of undulating patterns on the wall.

In thermodynamic terms, it was also observed that higher wave amplitudes and smaller wavelengths act synergistically to reduce the system's entropy generation. This behaviour is in consonance with the system's heat transfer characteristics. As the rate of heat transfer drops, so too do the temperature gradients within the fluid. This, in turn, weakens the forces driving natural convection, ultimately resulting in lower entropy generation. To provide a more comprehensive understanding, Figures 8 and 9 offer intricate visualizations, such as isotherms, streamlines, local entropy generation, and phase transition (*Cr*) contours. Figure 8 specifically focuses on how varying wave amplitudes impacts the system. An increase in wave amplitude tends to disrupt the homogeneity of solid blocks in the system, thereby elevating thermal resistance along the horizontal axis. The undulating waves also serve as physical barriers that impede fluid flow. However, this increase in surface area, brought about by the wave-like structures, can potentially augment the heat transfer rate, albeit in a complex manner.

Furthermore, as the amplitude of the waves increases, the *Cr* contours migrate upwards toward the colder wall, constricting the phase transition zone to a more confined space. Analysis of the local entropy generation reveals that entropy is predominantly generated along the vertical walls above heated surfaces and near the undulating peaks in proximity to both hot and cold regions of the solid blocks. While the increase in wave amplitude does not significantly alter the intensity of local entropy generation, it does result in a reduced spatial extent, leading to an overall decline in system entropy.

Figure 9 shows the role of wavelength in the system. A larger wavelength – which translates to fewer undulations – promotes a more favourable temperature gradient near heated and cooled regions within the blocks. This augmentation of the wavelength also expands the *Cr* region, thereby optimizing the utilization of the latent heat stored in nanoparticle cores for more effective heat transfer. Moreover, longer wavelengths lead to broader regions of intense entropy generation near undulating peaks. However, as the wavelength decreases, although the number of undulations rises, the region of significant entropy generation becomes more confined.

In terms of fluid dynamics, the streamlines are significantly influenced by the wavelength. Higher wavelengths cause the streamlines to more accurately replicate the form of the wavy wall. This leads to less fluid being trapped in the undulations, which in turn enhances the heat transfer efficiency via more robust natural convection flows.

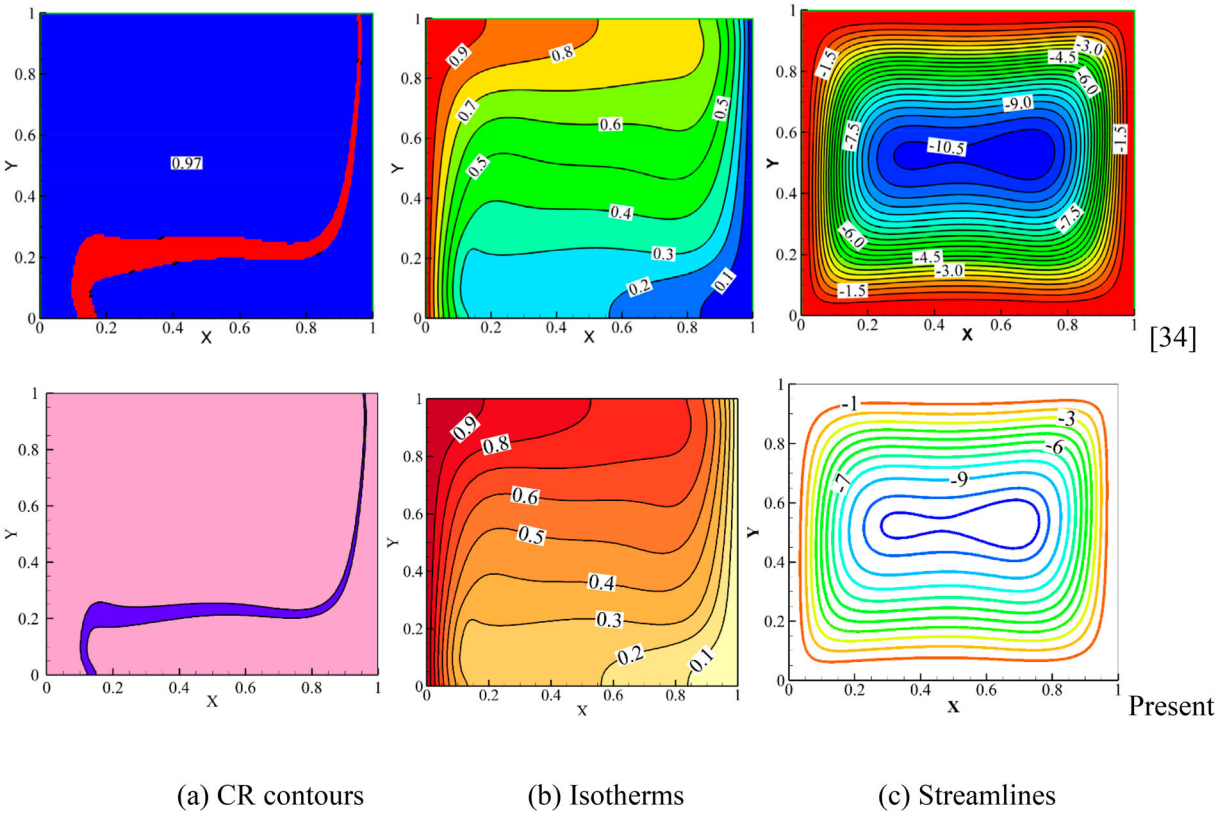

Figure 5. Comparison between the CR, isotherms, and streamlines of the present study and those of [34] for heat transfer of NEPCM suspensions in a square cavity for Ra $= 10^5$, $\theta_f = 0.3$, Pr $= 6.2$, Ste $= 0.3$, $\lambda_0 = 0.33$, $Nv = 3$, $Nc = 3$, and $\varphi = 0.05$, and $\rho_p/\rho_f = 0.9$. (a) CR contours; (b) Isotherms; (c) Streamlines.

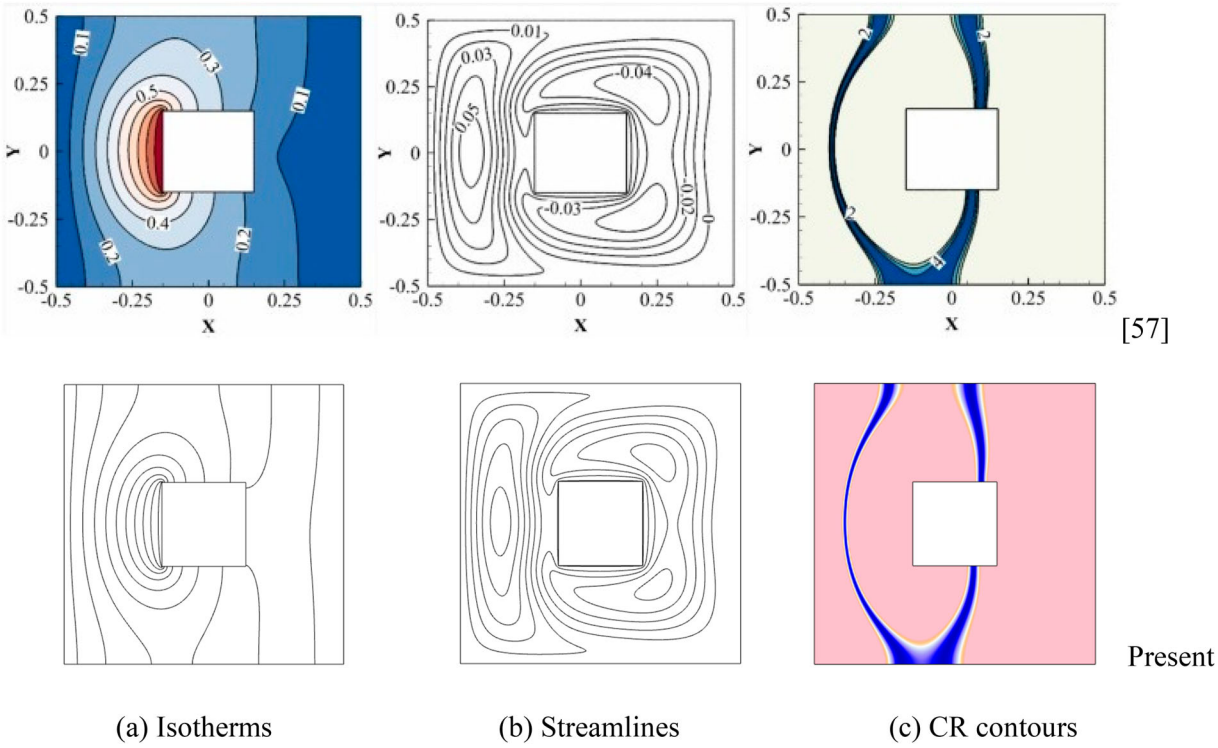

Figure 6. Comparison between the CR, isotherms, and streamlines of the present study and those of [57] for heat transfer of NEPCM suspensions in a complex cavity for $Ha = 1$, $L = 0.3$, $\theta_f = 0.25$, Pr $= 6.2$, Ra $= 10^3$, $Ste = 0.3$, $\varphi = 0.04$, $\delta = 0.05$, $Nv = 12.5$, $Nc = 23.8$, $\lambda_0 = 0.33$, and $\rho_p/\rho_f = 0.9$. (a) Isotherms; (b) Streamlines; (c) CR contours.

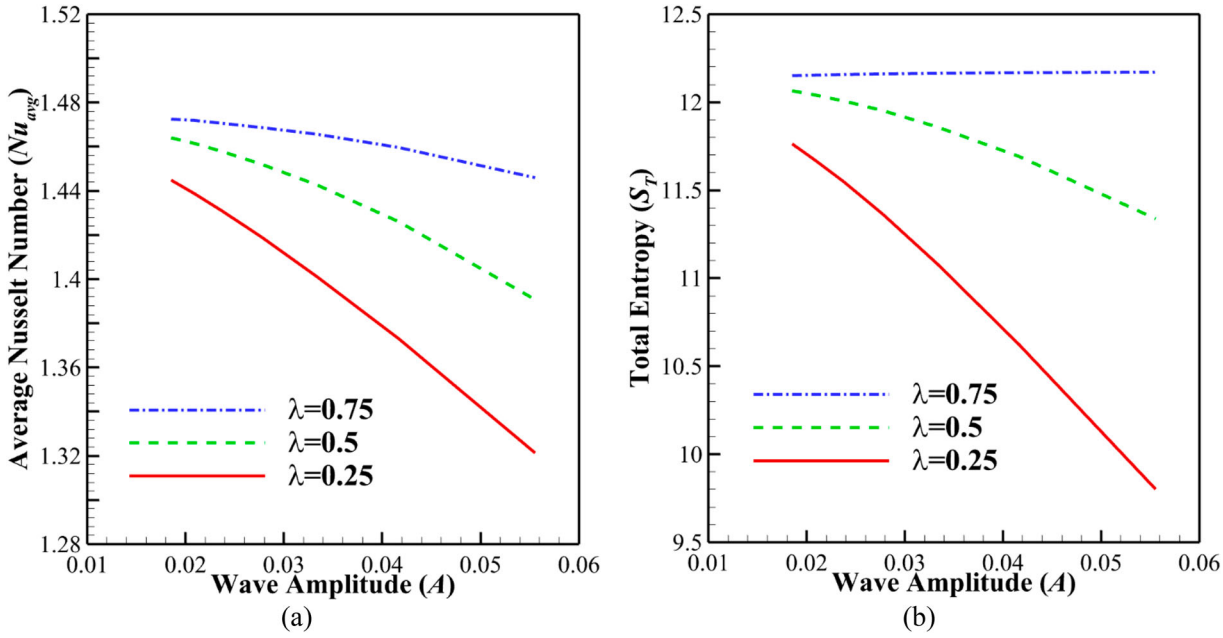

Figure 7. Effect of wave amplitude and wavelength on the (a) Average Nusselt number and (b) Total entropy.

Figure 10 explores the interplay between Ra and R_k and their influence on two key metrics: the average Nusselt number (Nu_{avg}) and the overall entropy generation (S_T). The Rayleigh number characterizes the driving force behind natural convection, while the thermal conductivity ratio represents the ratio of the thermal conductivities between the solid wall and the fluid. As illustrated, elevating the Rayleigh number boosts both heat transfer rates and entropy generation within the system. This trend of results for Ra is in agreement with the study of Pasha et al. [36] who also observed the significance of Rayleigh number on increase of heat transfer rate and entropy generation in exothermic reaction natural convection of NEPCM suspensions.

An increase of Rayleigh number increases the buoyancy forces driving the natural convection flows. Thus, as Ra increases the strength of the convection flow improves. The faster the fluid moves the better it circulates the absorbed heat inside the enclosure and releases the heat to the cold wall. Interestingly, the influence of the Rayleigh number on Nu_{avg} becomes particularly pronounced when the thermal conductivity ratio is high ($R_k = 10$). In scenarios where R_k is low, substantial conductive thermal resistance exists within the solid wall, thereby impeding effective heat transfer to the fluid. Under these conditions, an increase in the Rayleigh number, although enhancing convective heat transfer within the fluid, fails to substantially improve Nu_{avg}. Conversely, when R_k is high, the solid wall's thermal conductivity improves considerably, enabling more efficient heat transfer into the fluid-filled enclosure. Here, the Rayleigh number gains greater leverage in affecting both entropy generation and heat transfer.

To quantify this, Figure 10 shows that for $R_k = 10$, Nu_{avg} increases from approximately 0.78 to 1.3 for $Ra = 10^5$ marking about a 66% improvement in the heat transfer. In contrast, when R_k is only 1, Nu_{avg} improves merely from 0.3 to 0.4 at the same Ra value, representing only a 33% increase. If we consider a constant Ra of 10^5, elevating R_k from 1 to 10 results in Nu_{avg} soaring from 0.4 to 1.3, an impressive 69% uptick in heat transfer effectiveness.

Figure 11 complements this data by offering contour maps for thermal conductivity ratios of $R_k = 1$, 5, and 10. When R_k is minimal ($R_k = 1$), the temperature distribution across the fluid is almost linear from left to right, signalling weak convective flows. However, as R_k increases, temperature gradients become more concentrated near the lower-left and upper-right corners, corresponding to the hot and cold boundary conditions, respectively. This suggests that higher R_k values amplify convective currents within the fluid, as evidenced by the increasing magnitude of the streamlines depicted in Figure 11.

Interestingly, varying R_k has a relatively minor impact on phase transition maps (Cr). An increase in R_k nudges the Cr contours slightly toward the colder wall. This movement suggests that a higher R_k minimizes the temperature differential between the cold wall and both the fluid and adjacent solid blocks. Furthermore, while an increase in R_k does not shift the location of high-entropy-generating regions, it does intensify their magnitudes. This escalation can be attributed to the enhanced heat transfer rates fostered by higher R_k values, which in turn exacerbate temperature gradients and, hence, contribute to greater entropy generation.

Figures 12 and 13 delve into the nuanced effects of wavelength (λ) and amplitude (A) on the average Nusselt number (Nu_{avg}) and total entropy generation (S_T), all considered across a range of Rayleigh

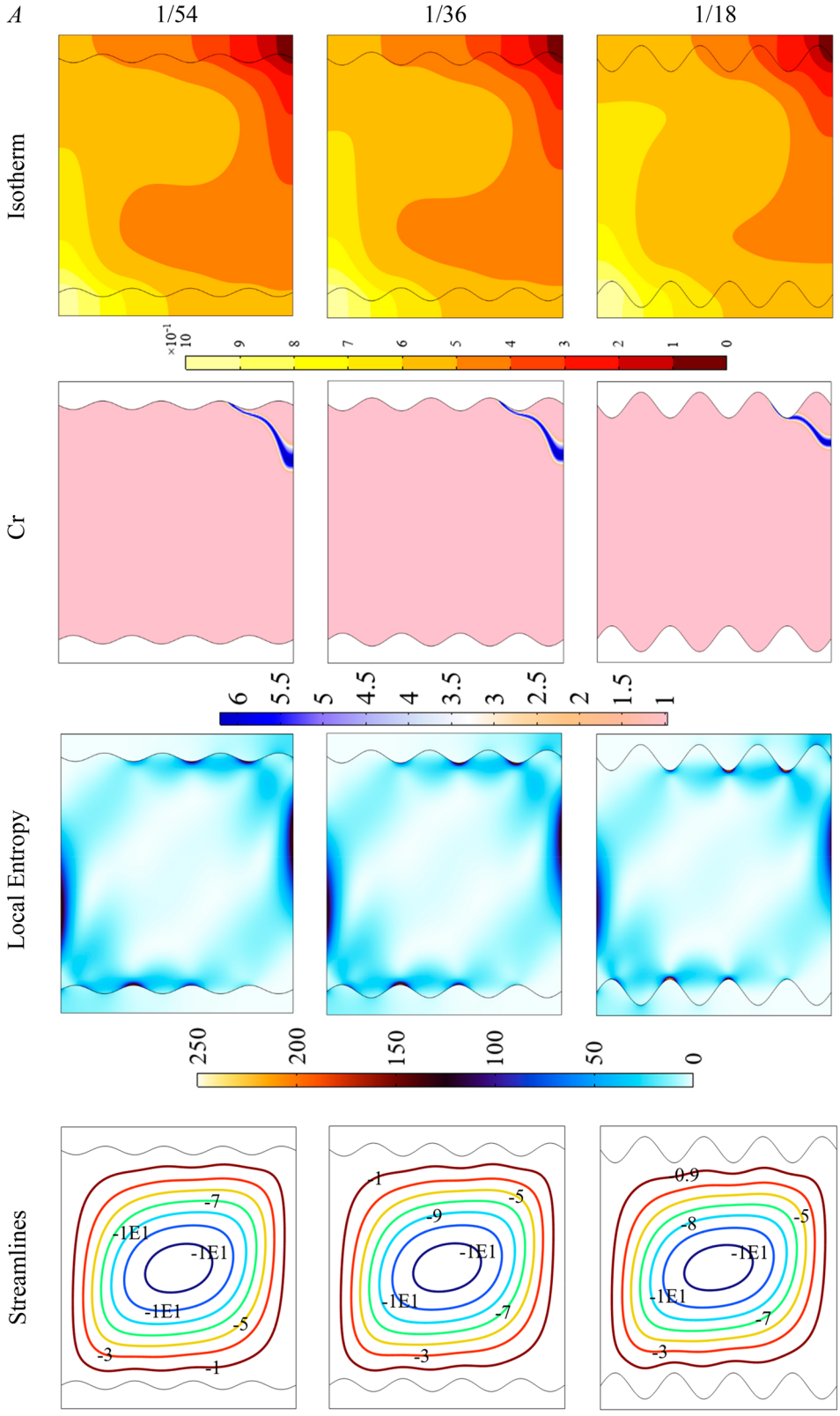

Figure 8. The isotherms (first row), CR contours (second row), entropy generation (third row), and streamlines (fourth row) for selected wave amplitudes (*A*).

numbers (Ra). The Rayleigh number serves as a gauge for the relative importance of convective heat transfer within the fluid. The wavy wall configuration is a particular focus here, as it introduces geometric complexities that can either enhance or hinder heat transfer and entropy generation. When considering wavelength, we observe that an increase in λ generally enhances Nu_{avg}, but this trend exhibits an exception at low Rayleigh numbers. In these low Ra regimes, conduction overwhelmingly dominates heat

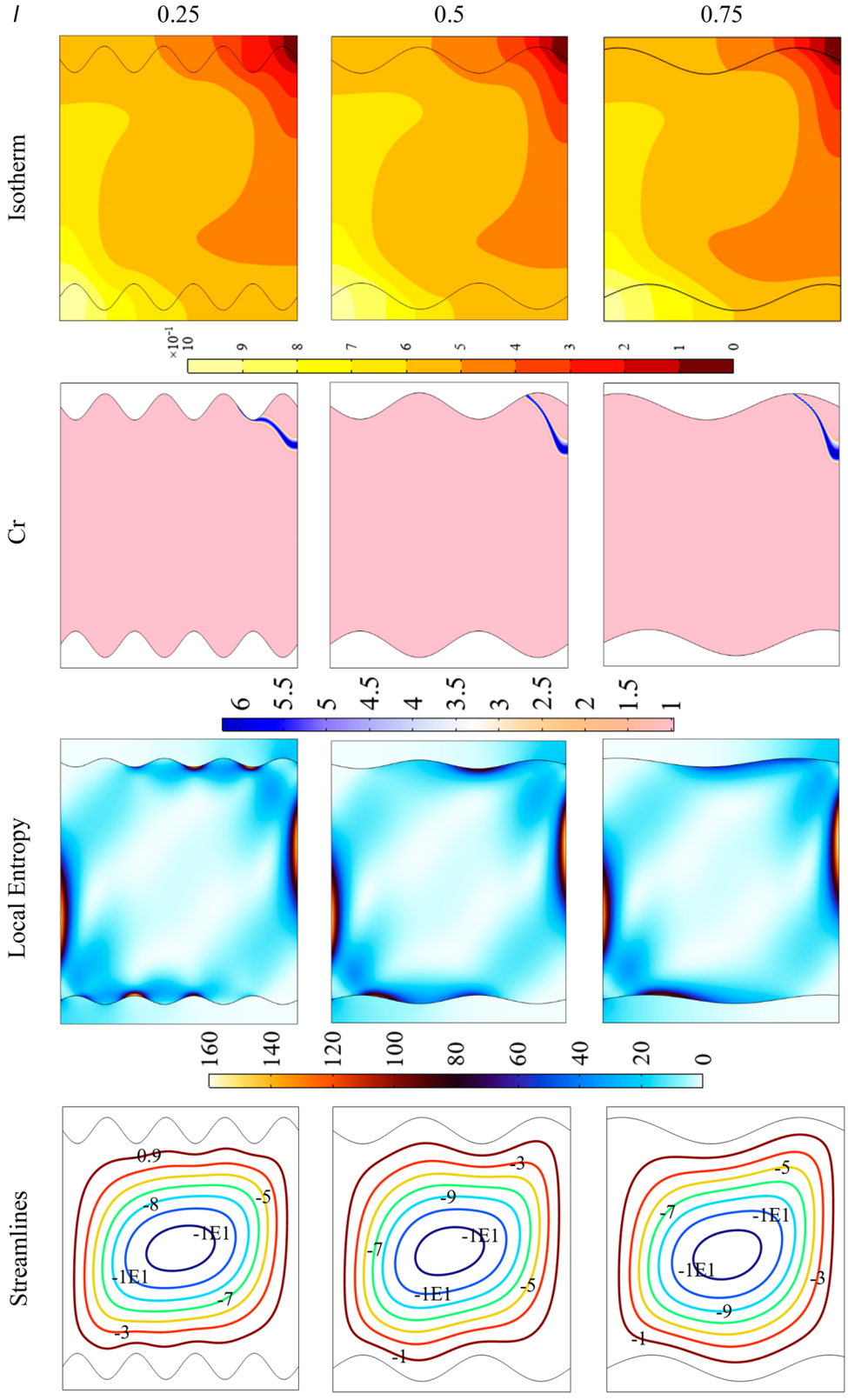

Figure 9. The isotherms (first row), CR contours (second row), entropy generation (third row), and streamlines (fourth row) for selected values of wavelength (λ).

transfer within the enclosure. Under such conditions, a wall with a high number of smaller waves (low λ) increases the effective surface area for heat transfer but introduces spatial inhomogeneities that affect the heat transfer in the horizontal direction. As a result, the lowest Nusselt number can be seen for case of $\lambda = 0.25$.

As the Rayleigh number escalates, convective heat transfer gains prominence. For walls with numerous small waves (low λ), the undulating surface introduces multiple restrictions or chocking points for both conduction within the blocks and fluid flow along the top and bottom walls. Thus, surfaces with fewer, larger undulations (higher λ values) are more conducive to

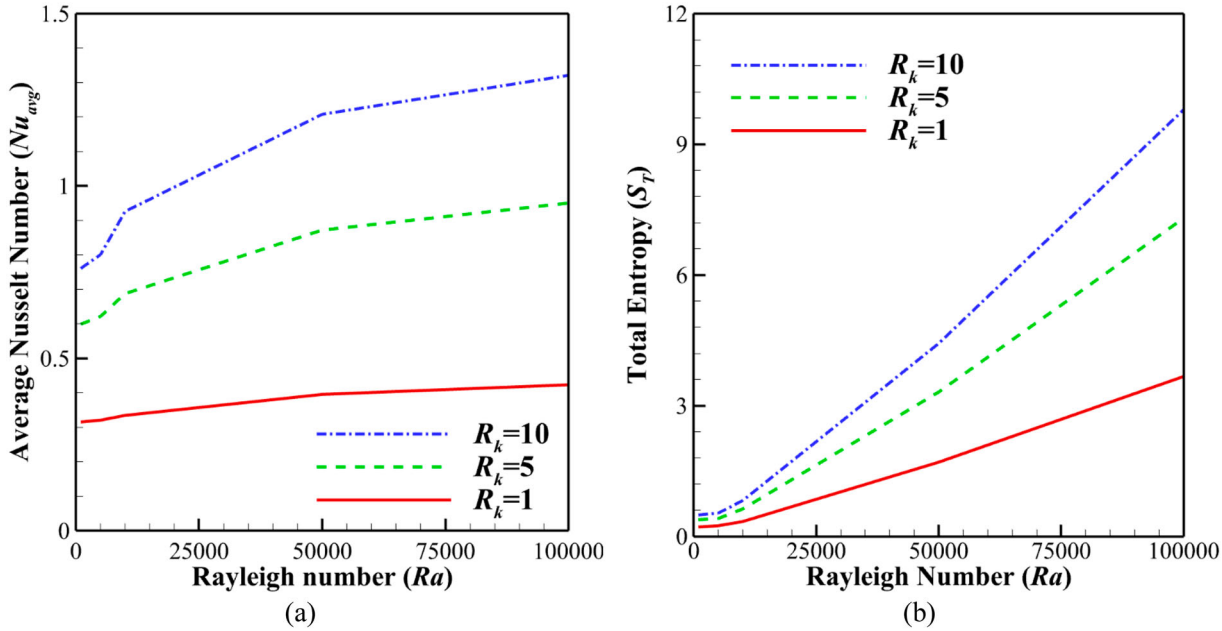

Figure 10. Effect of Rayleigh number (Ra) and thermal conductivity ratio (R_k) on (a) Average Nusselt number and (b) Total entropy.

effective heat transfer. Furthermore, elevating the wave number also inflates total entropy generation, a consequence of heightened heat transfer rates and increased thermal gradients within the enclosure.

In terms of wave amplitude (A), Figure 13 shows that its influence varies with the Rayleigh number. At high Ra values (e.g. Ra $= 10^5$), elevating (A) typically curtails Nu_{avg} which is in agreement with findings of Tayebi et al. [58]. However, for lower Ra regimes, exceptions to this trend manifest. In extremely low Ra scenarios, where conduction is dominant, higher amplitude augments the surface area for heat transfer between the solid blocks and the fluid. Nonetheless, increased amplitude also narrows the conduits for heat to flow within the blocks, creating an unfavourable setup for efficient heat transfer. Consequently, wave amplitude's influence on Nu_{avg} is somewhat ambiguous at low Rayleigh numbers.

For moderate Ra values, increasing amplitude yields a mixed bag of effects. On the one hand, higher amplitude traps fluid within the undulations, hindering fluid flow. On the other hand, the enlarged surface area promotes better heat transmission between the solid block and the fluid. Therefore, a range of behaviours is exhibited for intermediate Rayleigh numbers.

In high Ra scenarios, the convective flow becomes substantially more potent, and effective heat transmission between the solid blocks and the fluid is achieved. Here, pronounced undulations introduced by high amplitude are counterproductive, impeding the fluid flow and hence diminishing the convective heat transfer. For instance, halving the amplitude from 1/18 (0.056) to 1/36 (0.028) led to an 9.2% increase in Nu_{avg}, from 1.3 to 1.42 at Ra $= 10^5$. It is also noteworthy that reducing A consistently elevates total entropy generation (S_T) across all Rayleigh numbers examined.

Figure 14 elucidates the intricate relationship between fusion temperature (θ_f) and nanoparticle concentration (φ) in their collective impact on the average Nusselt number (Nu_{avg}) and total entropy generation (S_T). Importantly, this analysis involves the use of nano-enhanced phase change materials (NEPCMs) – nanoparticles with phase-changing cores that offer unique thermophysical properties.

In a scenario devoid of nanoparticles ($\varphi = 0$), varying the fusion temperature (θ_f) has a negligible impact on both (Nu_{avg}) and (S_T). However, as φ increases, the influence of θ_f becomes markedly significant. Specifically, an optimum fusion temperature around $\theta_f = 0.5$ emerges. When θ_f is elevated from 0.1 to 0.5 with 5% NEPCM concentration, Nu_{avg} improves by approximately 5%, climbing from 1.31 to 1.38. This is noteworthy as such an improvement is achieved without introducing additional materials. Moreover, the optimized combination of $\varphi = 0.05$ and $\theta_f = 0.5$ results in $Nu_{avg} = 1.38$ which offers a 12% enhancement in Nu_{avg} when compared to the baseline fluid with $\varphi = 0$ ($Nu_{avg} = 1.22$).

Interestingly, the presence of nanoparticles introduces a nuanced behaviour in entropy generation. At the optimum values of $\theta_f = 0.5$ and $\varphi = 0.05$, S_T diminishes to 6.1 compared to 9.1 for the host fluid $\varphi = 0$, representing a 33% reduction in entropy generation. This can be attributed to the phase-changing cores of the nanoparticles, which moderate local temperature gradients and thereby curtail overall entropy production.

Figure 15 further illuminates these phenomena by focusing on the local Nusselt number (Nu_Y) at the hot

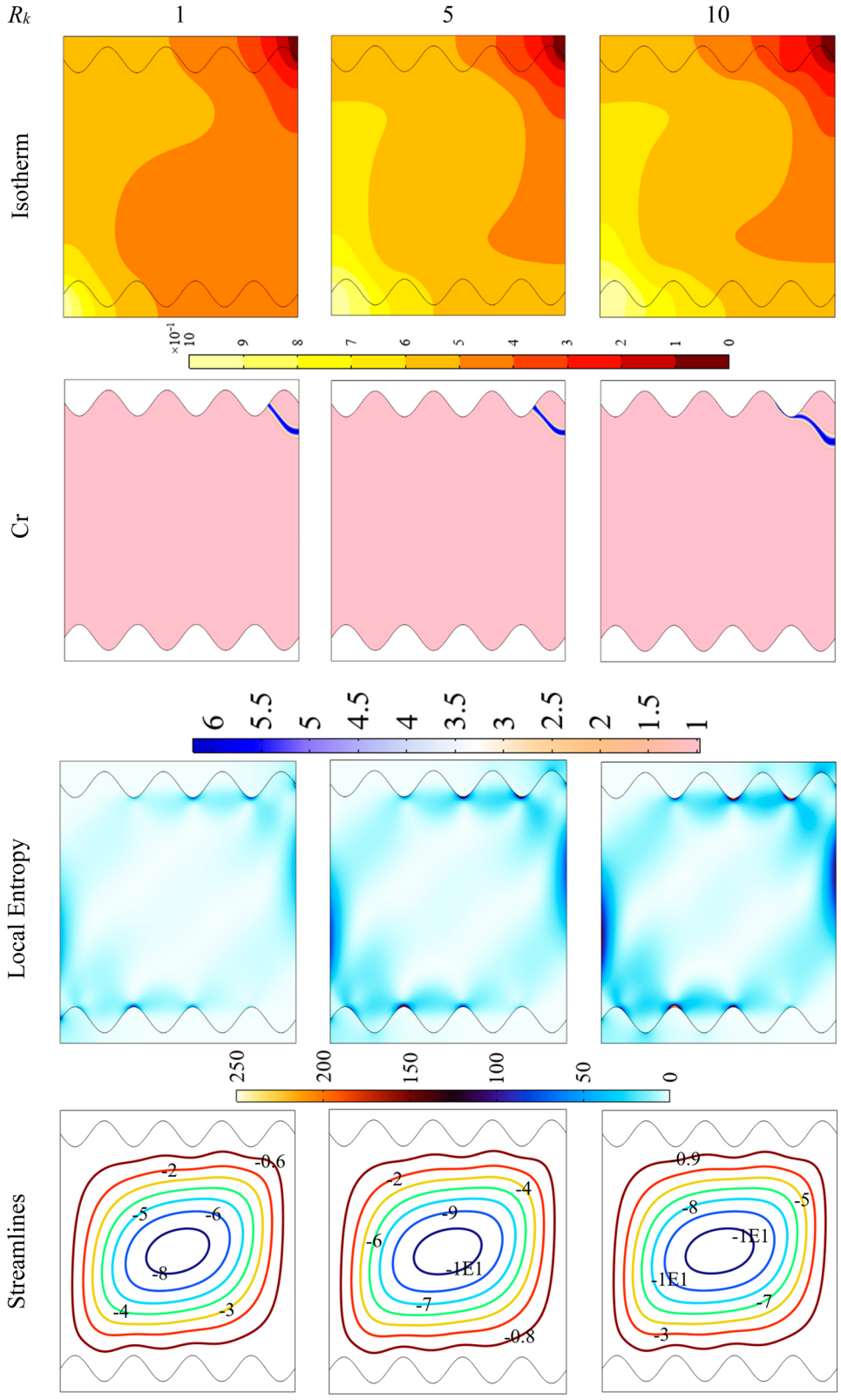

Figure 11. The isotherms (first row), Cr contours (second row), entropy generation (third row), and streamlines (fourth row) for selected values of R_k.

wall. The upper region, where the nanoparticle suspension meets the solid block, experiences sharp temperature gradients, resulting in a spike in Nu_Y. Moving downward along the wall, these gradients diminish rapidly. This decrease is driven by heat conduction into the block's interior, followed by heat dispersal into the nanoparticle suspension via the wavy surface. Consistent with Figure 14, both an increase in φ and θ_f bolster the local Nusselt number. Moreover, the curves for $\theta_f = 0.5$ and 0.7 are strikingly similar, signifying the existence of an optimal fusion temperature in that range. An increase of nanoparticles

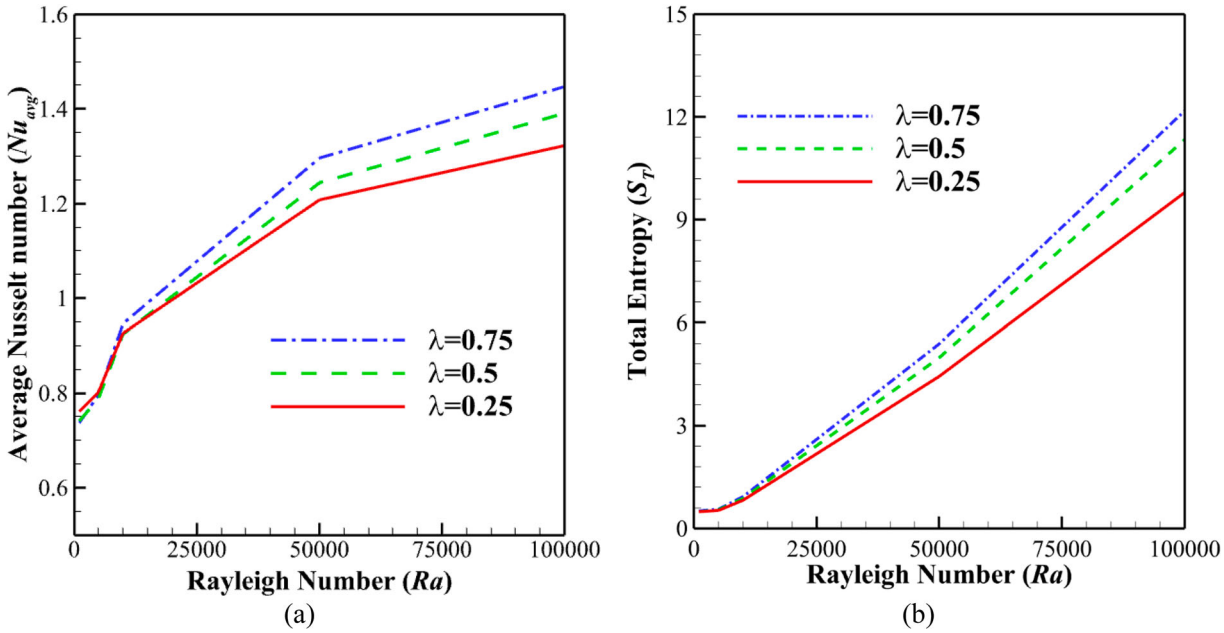

Figure 12. Effect of Rayleigh number (Ra) and wavelength (λ) on (a) Average Nusselt number and (b) Total entropy.

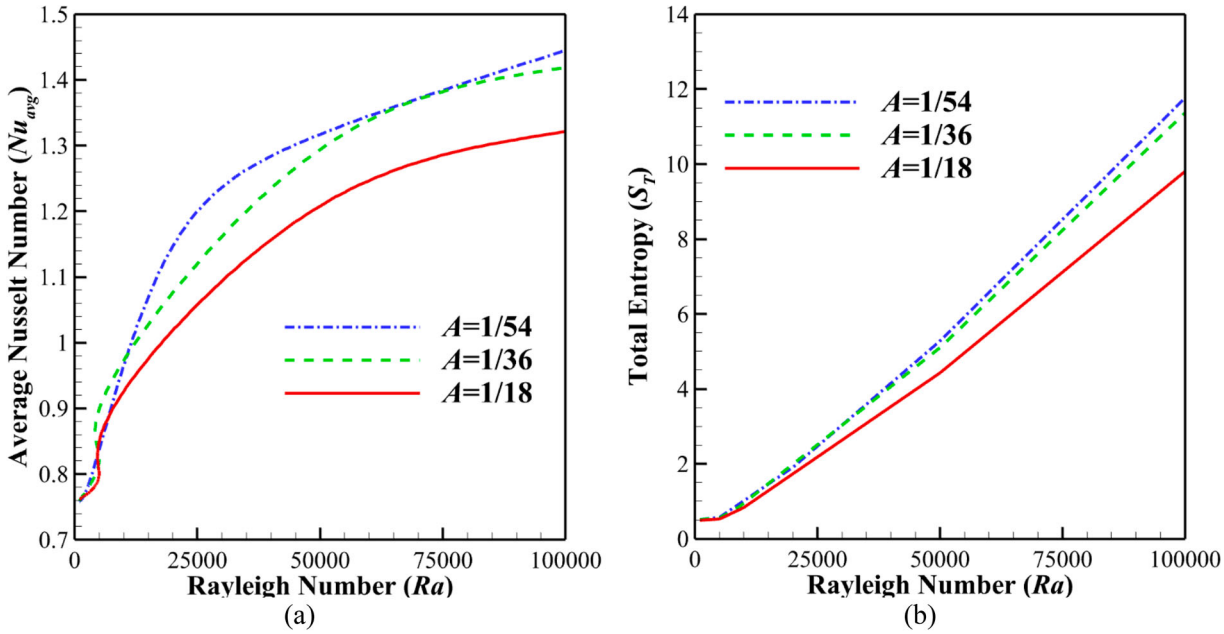

Figure 13. Effect of Rayleigh number (Ra) and wave amplitude (A) on (a) Average Nusselt number and (b) Total entropy.

concentration increases the average Nusselt number. This occurs because the nanoparticles transport heat in the form of latent heat, contributing to enhanced temperature gradients. Additionally, the presence of nanoparticles increases the thermal conductivity of the suspension, resulting in improved heat transfer within the enclosure and a higher Nusselt number.

Figure 16 explores contour maps that vary with fusion temperature. Increasing θ_f brings about significant changes in the contour of phase transitions (Cr), especially around θ_f, where the phase change of nanoparticles becomes a dominant factor. However, the alteration in θ_f has a minimal immediate impact on isotherms, local entropy generation, and fluid flow streamlines. The variation of θ_f influences the location of the phase transition region, which in turn affects the temperature and streamlines due to the localized changes in the fluid's heat capacity. The phase transition region, indicated by the Cr contour, primarily affects these factors indirectly by first modifying temperature contours, which subsequently influence entropy and fluid dynamics.

5. Conclusions

The contemporary research landscape in thermal sciences is replete with studies on heat transfer and entropy generation within complex enclosures. However, limited work has been dedicated to the investigation of these phenomena in wavy enclosures filled with

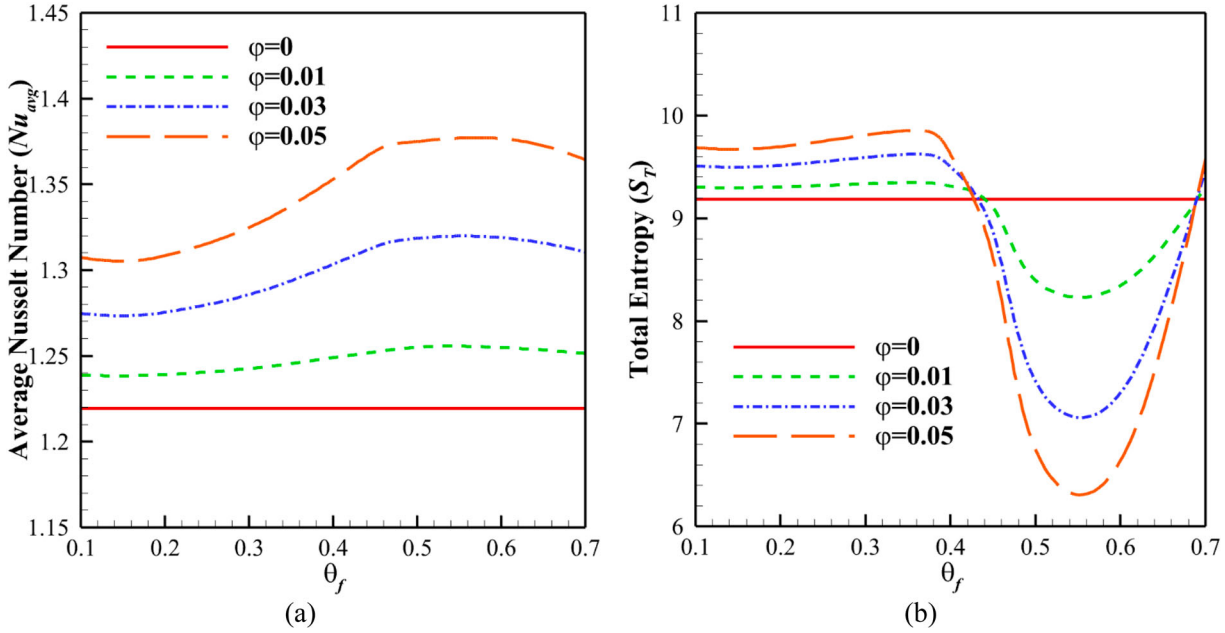

Figure 14. Effect of fusion temperature (θ_f) and nanoparticles concentration (φ) on (a) Average Nusselt number and (b) Total entropy.

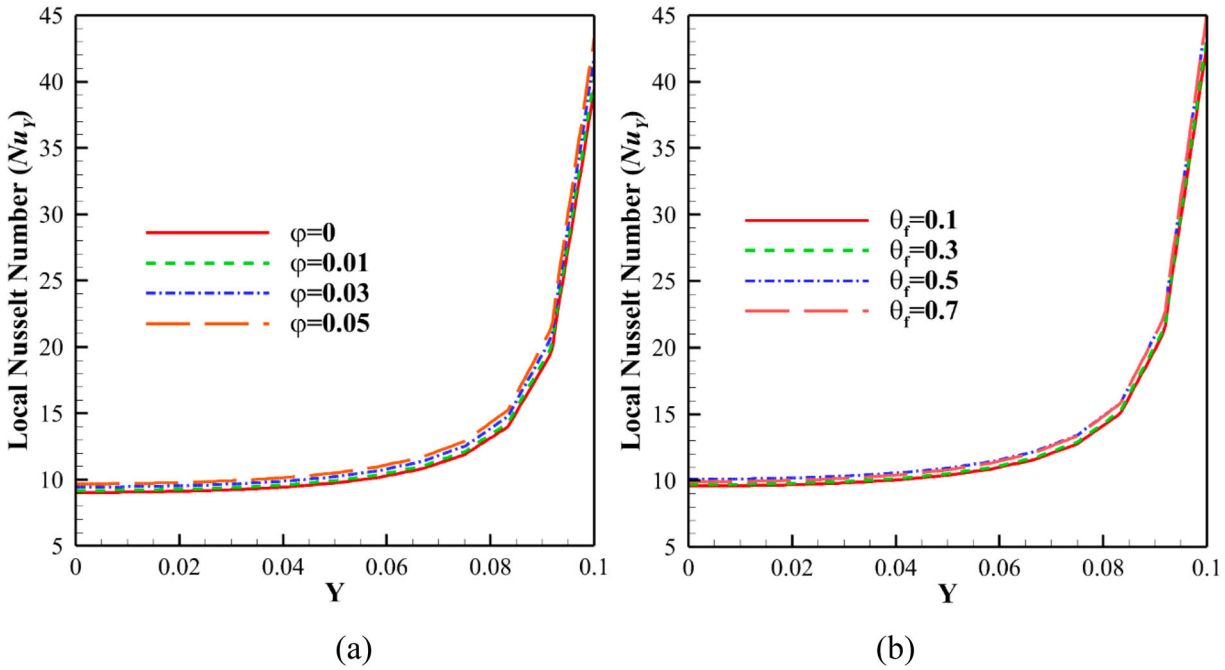

Figure 15. Local Nusselt number (Nu_Y) for various values of (a) nanoparticles concentration and (b) nanoparticles fusion temperature (θ_f).

NEPCM suspensions. The present study pioneers an analysis of conjugate heat transfer and entropy generation within a two-dimensional wavy enclosure filled with water-based NEPCM suspensions. A robust numerical methodology employing Galerkin's weighted finite element method solves the dimensionless governing equations. The simulation framework considers a multitude of non-dimensional parameters, including the Rayleigh number (Ra), thermal conductivity ratio (R_k), volume fraction of NEPCM particles (φ), and fusion temperature of nanoparticles (θ_f). The results are reported in the form of average Nusselt number and total entropy generation curves. Contours for isotherms, phase transitions, local entropy generation, and streamlines were also reported. Key outcomes can be summarized as:

1. Wave amplitude and wavelength show a decisive influence on heat transfer and entropy generation. Higher wave amplitudes and shorter wavelengths were found to decrease both heat transfer and entropy generation rates. Specifically, at higher frequencies of undulating patterns, Nu_{avg} declined more sharply.

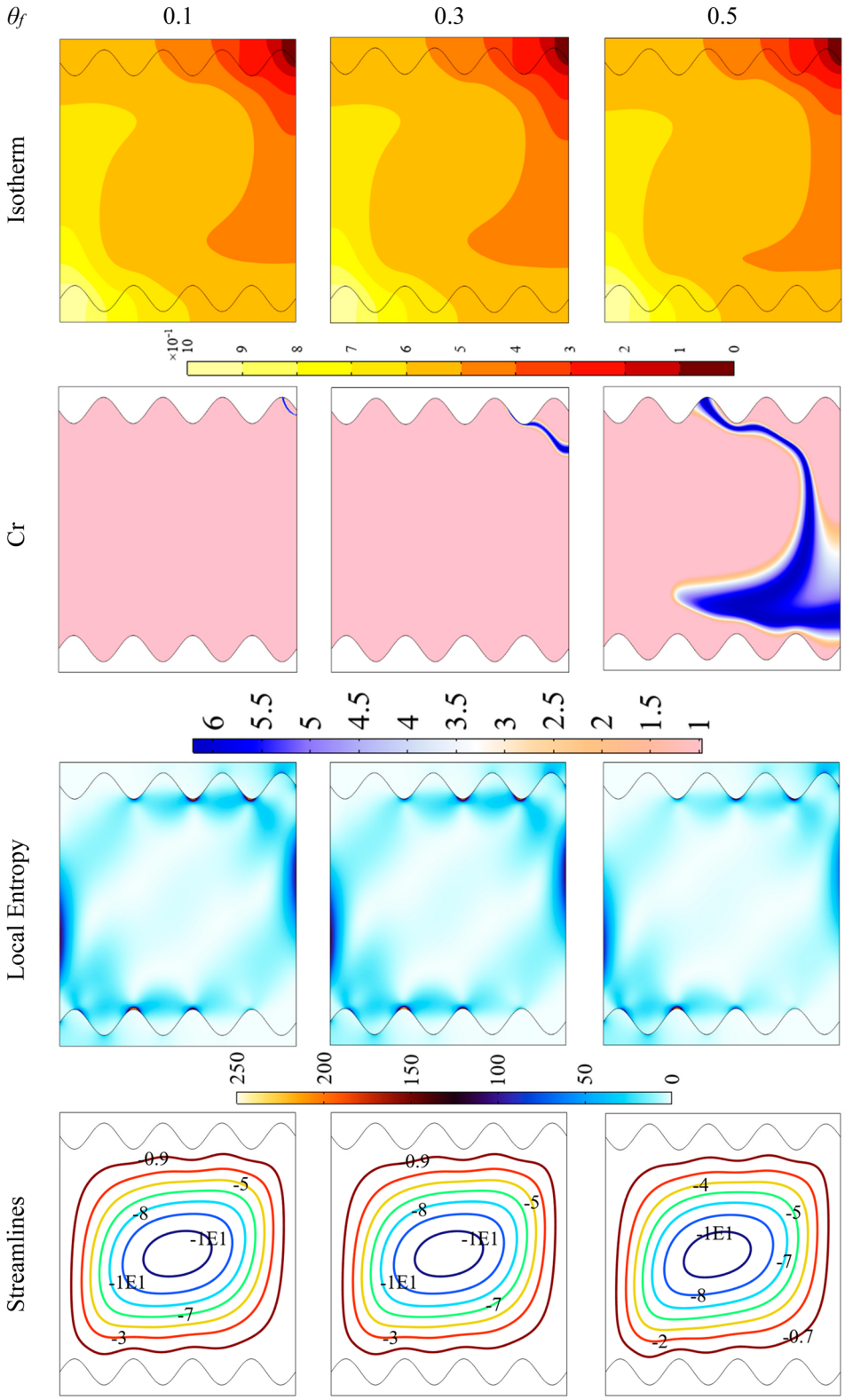

Figure 16. The isotherms (first row), Cr contours (second row), entropy generation (third row), and streamlines (fourth row) for selected values of θ_f.

2. Ra and R_k act in synergy to influence heat transfer and entropy generation. At $\mathrm{Ra} = 10^5$ and $R_k = 10$, Nu_{avg} rose by 66%, while a mere 33% improvement occurred at the same Ra but with $R_k = 1$. This highlighted the importance of wall thermal conductivity in affecting heat transfer efficiency.
3. The current research identified optimal nanoparticle concentration ($\varphi = 0.05$) and fusion temperature ($\theta_f = 0.5$) for the NEPCM suspensions, resulting in a 12% improvement in Nu_{avg} and a 33% reduction in entropy generation.
4. NEPCM particles altered the temperature gradients and, consequently, the entropy generation

within the system. An optimum fusion temperature and particle concentration led to reduced overall entropy generation, making the system more thermodynamically efficient.

Acknowledgements

The authors extend their appreciation to Umm Al-Qura University, Saudi Arabia for funding this research under grant number: 25UQU4310414GSSR01NI.

Disclosure statement

No potential conflict of interest was reported by the author(s).

Funding

This research work was funded by Umm Al-Qura University, Saudi Arabia under the grant number: 25UQU4310414GSSR01NI.

ORCID

Mehdi Ghalambaz http://orcid.org/0000-0001-8762-5510
Manuel Baro http://orcid.org/0000-0003-1665-8379

References

[1] Ghoghaei MS, Mahmoudian A, Mohammadi O, et al. A review on the applications of micro-/nano-encapsulated phase change material slurry in heat transfer and thermal storage systems. J Therm Anal Calorim. 2021;145:245–268. doi:10.1007/s10973-020-09697-6

[2] Albdour SA, Haddad Z, Sharaf OZ, et al. Micro/nano-encapsulated phase-change materials (ePCMs) for solar photothermal absorption and storage: fundamentals, recent advances, and future directions. Prog Energy Combust Sci. 2022;93:101037. doi:10.1016/j.pecs.2022.101037

[3] Huang Y, Stonehouse A, Abeykoon C. Encapsulation methods for phase change materials–a critical review. Int J Heat Mass Transfer. 2023;200:123458. doi:10.1016/j.ijheatmasstransfer.2022.123458

[4] Mehrjardi SAA, Khademi A, Ushak S, et al. Melting process of various phase change materials in presence of auxiliary fluid with sinusoidal wall temperature. J Energy Storage. 2022;52:104779. doi:10.1016/j.est.2022.104779

[5] Sadeghi HM, Babayan M, Chamkha A. Investigation of using multi-layer PCMs in the tubular heat exchanger with periodic heat transfer boundary condition. Int J Heat Mass Transfer. 2020;147:118970. doi:10.1016/j.ijheatmasstransfer.2019.118970

[6] Miroshnichenko I, Sheremet M. Turbulent natural convection heat transfer in rectangular enclosures using experimental and numerical approaches: a review. Renewable Sustainable Energy Rev. 2018;82:40–59. doi:10.1016/j.rser.2017.09.005

[7] Das D, Roy M, Basak T. Studies on natural convection within enclosures of various (non-square) shapes–a review. Int J Heat Mass Transfer. 2017;106:356–406. doi:10.1016/j.ijheatmasstransfer.2016.08.034

[8] Rafeek KVM, Reddy GJ, Ragoju R, et al. Impact of throughflow and coriolis force on the onset of double-diffusive convection with internal heat source. Coatings. 2022;12(8):1096. doi:10.3390/coatings12081096

[9] Muthukumar S, Sureshkumar S, El-Sapa S, et al. Impacts of uniform and sinusoidal heating in a nanofluid saturated porous chamber influenced by the thermal radiation and the magnetic field. Numer Heat Transfer, Part A. 2023;84(5):488–506. doi:10.1080/10407782.2022.2137072

[10] Reddy NK, Swamy HK, Sankar M, et al. MHD convective flow of Ag–TiO2 hybrid nanofluid in an inclined porous annulus with internal heat generation. Case Stud Therm Eng. 2023;42:102719. doi:10.1016/j.csite.2023.102719

[11] Baïri A, Zarco-Pernia E, De María J-MG. A review on natural convection in enclosures for engineering applications. The particular case of the parallelogrammic diode cavity. Appl Therm Eng. 2014;63(1):304–322. doi:10.1016/j.applthermaleng.2013.10.065

[12] Alsabery AI, Abosinnee AS, Al-Hadraawy SK, et al. Convection heat transfer in enclosures with inner bodies: a review on single and two-phase nanofluid models. Renewable Sustainable Energy Rev. 2023;183:113424. doi:10.1016/j.rser.2023.113424

[13] Azzouz R, Hamida MBB. Natural convection in a circular enclosure with four cylinders under magnetic field: application to heat exchanger. Processes. 2023;11(8):2444. doi:10.3390/pr11082444

[14] Azizul FM, Alsabery AI, Hashim I, et al. MHD mixed convection and heatlines approach of nanofluids in rectangular wavy enclosures with multiple solid fins. Sci Rep. 2023;13(1):9660. doi:10.1038/s41598-023-36297-9

[15] Massoudi MD, Hamida MBB. Combined impacts of square fins fitted wavy wings and micropolar magnetized-radiative nanofluid on the heat sink performance. J Magn Magn Mater. 2023;574:170655. doi:10.1016/j.jmmm.2023.170655

[16] Shao W, Nayak M, El-Sapa S, et al. Entropy optimization of non-Newtonian nanofluid natural convection in an inclined U-shaped domain with a hot tree-like baffle inside and considering exothermic reaction. J Taiwan Inst Chem Eng. 2023;148:104990. doi:10.1016/j.jtice.2023.104990.

[17] John B, Senthilkumar P, Sadasivan S. Applied and theoretical aspects of conjugate heat transfer analysis: a review. Arch Comput Methods Eng. 2019;26:475–489. doi:10.1007/s11831-018-9252-9

[18] Errera M-P, Moretti R, Mayeur J, et al. A numerical predictive model for conjugate heat transfer with radiation. Int J Heat Mass Transfer. 2020;160:120155. doi:10.1016/j.ijheatmasstransfer.2020.120155

[19] Alhashash A, Saleh H. Enhancement of conjugate heat transfer in an enclosure by utilizing water and nano encapsulated phase change materials with active cylinder. J Energy Storage. 2023;66:107422. doi:10.1016/j.est.2023.107422

[20] Abdi M, Chaib K, Menouer A, et al. A natural convection conjugate heat transfer of Nano-Encapsulated Phase Change Materials (NEPCMs) in an inclined blocked square enclosure. Numer Heat Transfer, Part A. 2023;84(6):604–625. doi:10.1080/10407782.2022.2153769

[21] Swamy HK, Reddy NK, Sankar M, et al. Conjugate heat transfer of aqueous hybrid nanoliquid between coaxial cylinders subjected to magnetic field. Int J Thermofluids. 2023;17:100299. doi:10.1016/j.ijft.2023.100299

[22] Tasnim S, Mitra A, Saha H, et al. MHD conjugate natural convection and entropy generation of a nanofluid filled square enclosure with multiple heat-generating elements in the presence of Joule heating. Res Eng. 2023;17:100993. doi:10.1016/j.rineng.2023.100993

[23] Chatterjee D, Biswas N, Manna NK, et al. Magneto-nanofluid flow in cylinder-embedded discretely heated-cooled annular thermal systems: conjugate heat transfer and thermodynamic irreversibility. J Magn Magn Mater. 2023;569:170442. doi:10.1016/j.jmmm.2023.170442

[24] Al-Chlaihawi KK, Alaydamee HH, Faisal AE, et al. Newtonian and non-Newtonian nanofluids with entropy generation in conjugate natural convection of hybrid nanofluid-porous enclosures: a review. Heat Transfer. 2022;51(2):1725–1745. doi:10.1002/htj.22372

[25] Reddy PBA, Salah T, Jakeer S, et al. Entropy generation due to magneto-natural convection in a square enclosure with heated corners saturated porous medium using Cu/water nanofluid. Chin J Phys. 2022;77:1863–1884. doi:10.1016/j.cjph.2022.01.012

[26] Dogonchi A, Chamkha AJ, Ganji D. A numerical investigation of magneto-hydrodynamic natural convection of Cu–water nanofluid in a wavy cavity using CVFEM. J Therm Anal Calorim. 2019;135(4):2599–2611. doi:10.1007/s10973-018-7339-z

[27] Fayz-Al-Asad M, Alam MN, Rashad A, et al. Impact of undulation on magneto-free convective heat transport in an enclosure having vertical wavy sides. Int Commun Heat Mass Transfer. 2021;127:105579. doi:10.1016/j.icheatmasstransfer.2021.105579

[28] Alrowaili D, Ahmed SE, Elshehabey HM, et al. Magnetic radiative buoyancy-driven convection of MWCNTs-C2H6O2 power-law nanofluids in inclined enclosures with wavy walls. Alexandria Eng J. 2022;61(11):8677–8689. doi:10.1016/j.aej.2022.01.073

[29] Abdulkadhim A, Hamzah HK, Ali FH, et al. Effect of heat generation and heat absorption on natural convection of Cu-water nanofluid in a wavy enclosure under magnetic field. Int Commun Heat Mass Transfer. 2021;120:105024. doi:10.1016/j.icheatmasstransfer.2020.105024

[30] Mandal DK, Biswas N, Manna NK, et al. Magneto-hydrothermal performance of hybrid nanofluid flow through a non-Darcian porous complex wavy enclosure. Eur Phys J Spec Top. 2022;231(13–14):2695–2712. doi:10.1140/epjs/s11734-022-00595-6

[31] Abdulkadhim A, Abed IM, Said NM. Magnetohydrodynamics thermogravitational convective in a novel I-shaped wavy-walled enclosure considering various inner hot pipe locations. J Therm Anal Calorim. 2022;147:7961–7990.

[32] Afsana S, Molla MM, Nag P, et al. MHD natural convection and entropy generation of non-Newtonian ferrofluid in a wavy enclosure. Int J Mech Sci. 2021;198:106350. doi:10.1016/j.ijmecsci.2021.106350

[33] Öztop HF, Estellé P, Yan W-M, et al. A brief review of natural convection in enclosures under localized heating with and without nanofluids. Int Commun Heat Mass Transfer. 2015;60:37–44. doi:10.1016/j.icheatmasstransfer.2014.11.001

[34] Ghalambaz M, Chamkha AJ, Wen D. Natural convective flow and heat transfer of nano-encapsulated phase change materials (NEPCMs) in a cavity. Int J Heat Mass Transfer. 2019;138:738–749. doi:10.1016/j.ijheatmasstransfer.2019.04.037

[35] Ghalambaz M, Mozaffari M, Yazdani S, et al. Conjugate entropy generation and heat transfer of a dilute suspension of nano-encapsulated phase change material in a partially heated wall cavity. Rep Mech Eng. 2023;4(1):175–192. doi:10.31181/rme040115092023g

[36] Pasha AA, Tayebi T, MottahirAlam M, et al. Efficacy of exothermic reaction on the thermal-free convection in a nano-encapsulated phase change materials-loaded enclosure with circular cylinders inside. J Energy Storage. 2023;59:106522. doi:10.1016/j.est.2022.106522

[37] Hussain S, Ertam F, Hamida MBB, et al. Analysis of bio-convection and oxytactic microorganisms in a porous cavity with nano-enhanced phase change materials and quadrant heater: application of support vector regression based model. J Energy Storage. 2023;63:107059. doi:10.1016/j.est.2023.107059

[38] Sadeghi M, Chamkha AJ, Ali R, et al. Hydrothermal behavior of micro-polar nano-encapsulated phase change materials (NEPCMs) in an inclined L-shaped cavity. Case Stud Therm Eng. 2022;35:102039. doi:10.1016/j.csite.2022.102039

[39] Raizah Z, Aly AM. A rotating superellipse inside a hexagonalshaped cavity suspended by nano-encapsulated phase change materials based on the ISPH method. Int J Numer Methods Heat Fluid Flow. 2022;32(3):956–977. doi:10.1108/HFF-03-2021-0220

[40] Ahmed SE, Raizah ZA. Analysis of the entropy due to radiative flow of nano–encapsulated phase change materials within inclined porous prismatic enclosures: finite element simulation. J Energy Storage. 2021;40:102719. doi:10.1016/j.est.2021.102719

[41] Barlak S, Sara ON, Karaipekli A, et al. Thermal conductivity and viscosity of nanofluids having nanoencapsulated phase change material. Nanoscale Microscale Thermophys Eng. 2016;20(2):85–96. doi:10.1080/15567265.2016.1174321

[42] Ghalambaz M, Sheremet MA, Pop I. Free convection in a parallelogrammic porous cavity filled with a nanofluid using Tiwari and Das' nanofluid model. PLoS One. 2015;10(5):e0126486. doi:10.1371/journal.pone.0126486

[43] Ghalambaz M, Zadeh SMH, Mehryan S, et al. Analysis of melting behavior of PCMs in a cavity subject to a non-uniform magnetic field using a moving grid technique. Appl Math Model. 2020;77:1936–1953. doi:10.1016/j.apm.2019.09.015

[44] Sheikholeslami M, Vajravelu K. Nanofluid flow and heat transfer in a cavity with variable magnetic field. Appl Math Comput. 2017;298:272–282. doi:10.1016/j.amc.2016.11.025

[45] Chai L, Shaukat R, Wang L, et al. A review on heat transfer and hydrodynamic characteristics of nano/microen capsulated phase change slurry (N/MPCS) in mini/micro channel heat sinks. Appl Therm Eng. 2018;135:334–349. doi:10.1016/j.applthermaleng.2018.02.068

[46] Chen B, Wang X, Zeng R, et al. An experimental study of convective heat transfer with microencapsulated phase change material suspension: laminar flow in a circular tube under constant heat flux. Exp Therm Fluid Sci. 2008;32(8):1638–1646. doi:10.1016/j.expthermflusci.2008.05.008

[47] Khanafer K, Vafai K. A critical synthesis of thermophysical characteristics of nanofluids. Int J Heat Mass Transfer. 2011;54(19–20):4410–4428. doi:10.1016/j.ijheatmasstransfer.2011.04.048

[48] Seyf HR, Zhou Z, Ma H, et al. Three dimensional numerical study of heat-transfer enhancement by nano-encapsulated phase change material slurry in microtube heat sinks with tangential impingement. Int J Heat Mass Transfer. 2013;56(1–2):561–573. doi:10.1016/j.ijheatmasstransfer.2012.08.052

[49] Zaraki A, Ghalambaz M, Chamkha AJ, et al. Theoretical analysis of natural convection boundary layer heat and mass transfer of nanofluids: effects of size, shape and type of nanoparticles, type of base fluid and working

temperature. Adv Powder Technol. 2015;26(3):935–946. doi:10.1016/j.apt.2015.03.012

[50] Ghalambaz M, Doostani A, Izadpanahi E, et al. Phase-change heat transfer in a cavity heated from below: the effect of utilizing single or hybrid nanoparticles as additives. J Taiwan Inst Chem Eng. 2017;72:104–115. doi:10.1016/j.jtice.2017.01.010

[51] Selimefendigil F, Öztop HF, Chamkha AJ. MHD mixed convection and entropy generation of nanofluid filled lid driven cavity under the influence of inclined magnetic fields imposed to its upper and lower diagonal triangular domains. J Magn Magn Mater. 2016;406:266–281. doi:10.1016/j.jmmm.2016.01.039

[52] The finite element method for fluid dynamics. In: OC Zienkiewicz, RL Taylor, P Nithiarasu, editors. The finite element method for fluid dynamics, 7th ed. Oxford: Butterworth-Heinemann; 2014. p. iii.

[53] Kahveci K. Buoyancy driven heat transfer of nanofluids in a tilted enclosure. J Heat Transfer. 2010;132(6):062501. doi:10.1115/1.4000744

[54] Turan O, Sachdeva A, Chakraborty N, et al. Laminar natural convection of power-law fluids in a square enclosure with differentially heated side walls subjected to constant temperatures. J Non-Newtonian Fluid Mech. 2011;166(17):1049–1063. doi:10.1016/j.jnnfm.2011.06.003

[55] Ilis GG, Mobedi M, Sunden B. Effect of aspect ratio on entropy generation in a rectangular cavity with differentially heated vertical walls. Int Commun Heat Mass Transfer. 2008;35(6):696–703. doi:10.1016/j.icheatmasstransfer.2008.02.002

[56] Calcagni B, Marsili F, Paroncini M. Natural convective heat transfer in square enclosures heated from below. Appl Therm Eng. 2005;25(16):2522–2531. doi:10.1016/j.applthermaleng.2004.11.032

[57] Ghalambaz M, Yusaf T, Pop I, et al. Magnetohydrodynamic free convection of nano-encapsulated phase change materials between two square cylinders: mapping the thermal behavior using neural networks. Alexandria Eng J. 2024;89:110–124. doi:10.1016/j.aej.2024.01.035

[58] Tayebi T, El-Sapa S, Karimi N, et al. Double-diffusive natural convection with Soret/Dufour effects and energy optimization of nano-encapsulated phase change material in a novel form of a wavy-walled I-shaped domain. J Taiwan Inst Chem Eng. 2023;148:104873. doi:10.1016/j.jtice.2023.104873